Determination of the photoemission position in single-photon ionization with attosecond streaking spectroscopy

Feng Wang,[1] Qing Liao,[1,*] Kai Liu,[1] Meiyan Qin,[1] Xiaofan Zhang,[1] Qingbin Zhang,[2] Wei Cao,[2,†] Liang-Wen Pi,[3] Yueming Zhou,[2] and Peixiang Lu[4]

[1]*Hubei Key Laboratory of Optical Information and Pattern Recognition, Wuhan Institute of Technology, Wuhan 430205, China*

[2]*Wuhan National Laboratory for Optoelectronics and School of Physics, Huazhong University of Science and Technology, Wuhan 430074, China*

[3]*State Key Laboratory of Transient Optics and Photonics, Xi'an Institute of Optics and Precision Mechanics of CAS, Xi'an 710119, China*

[4]*Guangdong Intelligent Robotics Institute, Dongguan 523808, China*

(Received 12 September 2019; accepted 13 January 2021; published 29 January 2021)

Attosecond metrology can directly measure attosecond emission time of photoexcited electrons from matter, providing unprecedented understanding of transition processes of electrons from bound to continuum states. However, some fundamental details of the electron dynamics in the entire emission process upon photoexcitation still remain debatable or unknown. The photoemission time delays deduced from attosecond streaking spectroscopy originate from photoelectron propagation in the coupled Coulomb-laser fields, encoding the spatial and spectral information of electrons upon photoexcitation. Here we demonstrate that attosecond photoemission delays can be used to image picometer-resolved photoemission position via a classical model. The electronic dynamics in the laser-assisted single-photon ionization process is fully captured by a quantum path-integral model. We trace the imaged photoemission position to the average position of spatially coherent superposition of electron waves upon photoexcitation and, in particular, predict emission position coinciding with the orbital radius of the ground state of hydrogen-like atoms, in contrast with previous predictions.

DOI: 10.1103/PhysRevA.103.013115

Transition of electrons from bound states into continuum states is one of the most fundamental quantum processes. Using attosecond (as) streaking or attosecond interferometric spectroscopies, the transition phases have been successfully accessed in the measurements of photoemission time delays with resolutions up to a few attoseconds [1–3]. Precisely recording the temporal information of photoemission significantly advanced our understanding of different electronic dynamics, such as the shake-up excitation in neon and helium atoms [4–7], the preferential emission in asymmetric molecules [8–10], the spectral resonance shape [11], delay-dependence on the final-state angular momentum in continuum-continuum transitions [12], delays induced by final-state band dispersion [13,14], angular momentum of initial states [15] in solids, and so on.

However, some fundamental details of electronic dynamics in the photoionization process have been still in debate or unknown. Some elaborated classical models [16–18] were developed in order to reveal the underlying mechanism of the measured photoemission time delays for hydrogen-like targets, the photoemission process of which can be accurately quantum-mechanically simulated by solving the time-dependent Schrödinger equation (TDSE). While these classical models predict photoemission time delays in good agreement with quantum-mechanical simulations, they employed different initial conditions. The initial photoemission position is chosen to be near zero from the nuclear (averaged over an ensemble) [17] or dependent on the velocity [18], and both models assume the initial momentum to be the asymptotic one without the probing infrared (IR) femtosecond (fs) laser field. The initial momentum of a photoelectron (PE) in a Coulomb potential should be quite different from the asymptotic one, especially at low final electron energies [19]. The determination of initial conditions of photoemission is central to comprehensive insight into photoelectric effect and to fully capture the subsequent electron dynamics. It is also important to advance the application of attosecond metrology in temporal-spatial measurements on the attosecond-subangstrom scale and investigations of different electronic dynamics mentioned above at a higher quantitative level.

In attosecond streaking spectroscopy, the photoemission time delays are deduced from the extreme ultraviolet (XUV)-IR relative delay-dependent final kinetic-energy oscillations. Both the temporal shift and amplitude of the energy oscillation depend on the coupling of the Coulomb potential from which the PEs are emitted and the probing IR field [16]. This strong dependence can be used to determine the initial position and momentum of PEs at the birth time with the aid of theoretical models that are capable of describing the emission process at a quantitative level. In this paper, we demonstrate that PE propagation in the Coulomb-laser coupling fields can be described by a classical model, providing general insight into the

*liaoqing@wit.edu.cn
†weicao@hust.edu.cn

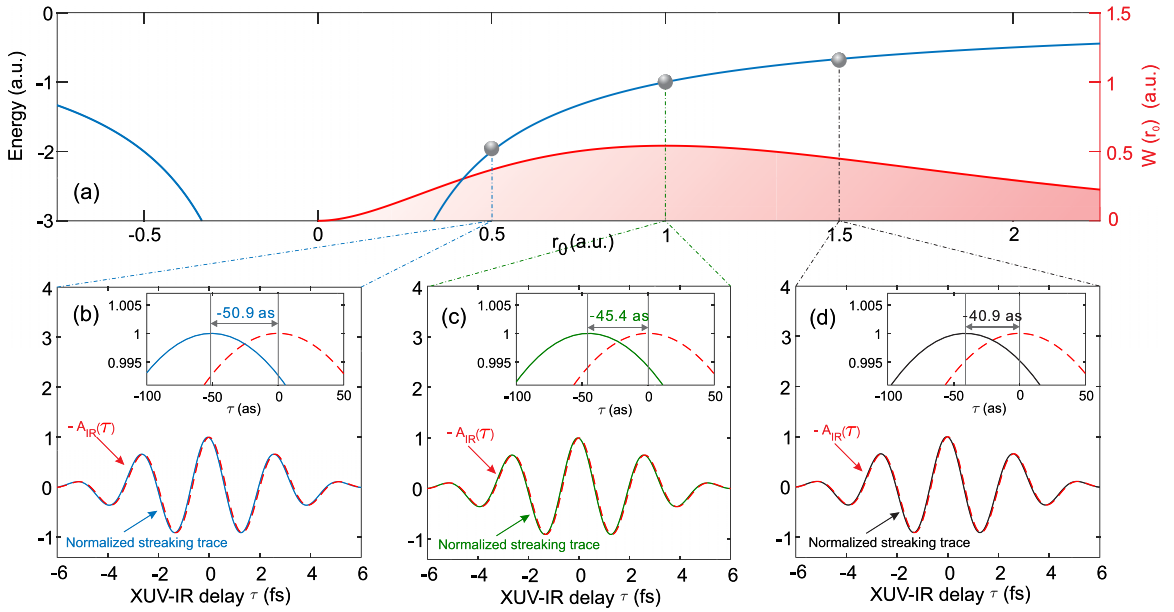

FIG. 1. (a) The Coulomb potential (blue solid lines) and radial probability density function $W(r_0)$ (red solid line) of the ground state of a H atom as a function of r_0. (b)–(d) Classically calculated normalized streaking traces of electron photoionized from the ground state of H atoms by absorption of one 25 eV photon in the presence of an IR laser pulse at different initial emission positions. The inset provides an enlarged view of the relative temporal shift between normalized streaking trace and the normalized negative IR vector potential $-A_{IR}(\tau)$ as a function of the XUV-IR relative delay τ (red dashed lines).

photoemission time delays. Taking the quantum-mechanically calculated photoemission time delays for the hydrogen (H) atom and singly charged helium ion (He^+) as prototypes, we validate this model and find that the initial emission position of PEs coincides with the orbital radii of their ground states within an uncertainty of a few picometers.

Neglecting the absorption process of an XUV photon, we only consider the propagation of PEs in the ionic Coulomb and the weak IR-laser coupling fields in a classical manner. In contrast with previous classical models in which the initial emission position is chosen first [17,18], we determine it by calibrating our classically calculated photoemission emission delays with quantum-mechanically ones. The trajectory of PE propagation is governed by the Newtonian equation (atomic units are used unless stated otherwise),

$$\frac{d^2 r_L}{dt^2} = -E_{IR}(t) - \frac{\partial V(r_L)}{\partial r_L}. \quad (1)$$

Here we only consider the propagation along the collinear direction of the linearly polarized IR laser field $E_{IR}(t)$ and the Coulombic field. The IR electric field and its vector potential are defined as $E_{IR}(t) = -\partial A_{IR}(t)/\partial t$ and $A_{IR}(t) = -(\varepsilon_{IR}/\omega_{IR})\cos^2(\pi t/T)\cos(\omega_{IR} t)$ with a total pulse duration $T = 5T_0$ ($T_0 = 2\pi/\omega_{IR}$), where ε_{IR} and ω_{IR} are the amplitude and frequency of the IR field, respectively. $V(r_L) = -Z/r_L$, with $Z = 1$ for the H atom and $Z = 2$ for the He^+ ion, is the ionic Coulomb potential. In our calculations, the initial velocity υ_0, depending on the initial emission position r_0, is given by

$$\upsilon_0 = \sqrt{2[\omega_X - I_p - V(r_0)]}, \quad (2)$$

according to law of conservation of energy, where I_p is the ionization potential and ω_X is the central XUV photon energy.

According to Eqs. (1) and (2), the electrons ionized from different initial positions have different initial velocities and thus undergo different Coulomb-laser coupling interaction in subsequent propagation, leading to different temporally shifted streaking traces. Solving Eq. (1) numerically, we obtain the final PE kinetic-energy oscillation with the birth time at different initial emission positions r_0. Note that, for sub-fs XUV pulses, the photoionization mainly arises near the center of the XUV pulse and the birth time equals the XUV-IR relative delay τ. Figures 1(b)–1(d) present the classically calculated normalized streaking traces of PEs freed by absorption of one 25 eV XUV photon from the ground state of H atoms in the presence of an 800 nm, 5×10^{11} W/cm^2 IR field at $r_0 = 0.5$, 1, and 1.5, respectively. They exhibit different temporal shifts, as compared with the negative IR vector potential $-A_{IR}(\tau)$ [see insets in Figs. 1(b)–1(d)].

We can accurately extract the photoemission time delays $\delta\tau$ by fitting these streaking traces into an analytic function with the same form as the IR vector potential, i.e., $f(\tau) = aA_{IR}(\tau - \delta\tau) + b$. As shown in the insets in Figs. 1(b)–1(d), with the initial position changing from 0.5 to 1.5, the absolute photoemission time delay reduces by 10 as. It is well understood that, since photoemission time delays deduced from attosecond streaking spectroscopy originates from the Coulomb-laser coupling [16–18], the larger r_0 means the weaker interaction of the PE with the coupling Coulomb-laser fields and thus the smaller absolute photoemission time delay. For $r_0 \to \infty$, there is no temporal shift for streaking traces.

To validate the above classical model, we compare the classical results with fully quantum-mechanical simulation results by numerically solving corresponding TDSE in spherical polar coordinates (see Appendix A). The XUV attosecond pulse is defined as $E_X(t) = E_{X0}(t)\cos(\omega_X t) =$

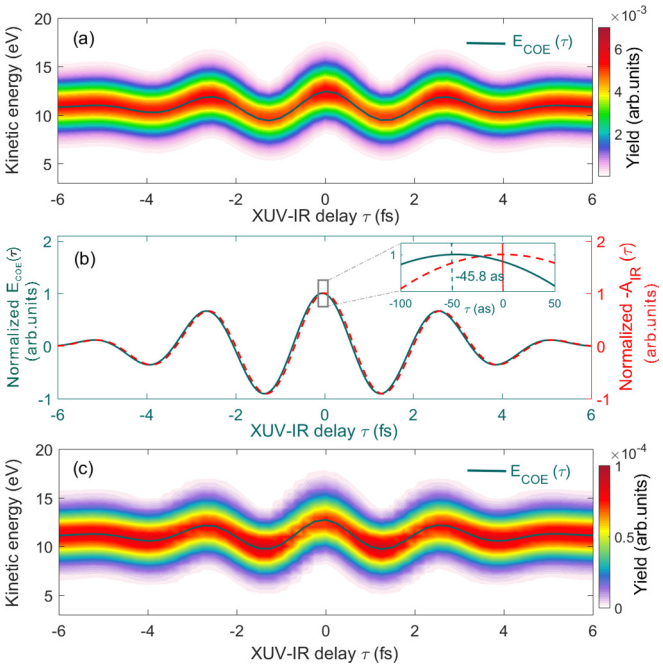

FIG. 2. (a) Quantum-mechanically calculated streaking spectrogram of PEs from the ground state of H atoms. Corresponding centers of energy $E_{\mathrm{COE}}(\tau)$ are represented by green solid line. (b) Normalized negative IR vector potential $-A_{\mathrm{IR}}(\tau)$ and normalized $E_{\mathrm{COE}}(\tau)$ as a function of τ. The inset provides an enlarged view of their relative temporal shift. (c) Streaking spectrogram and centers of energy $E_{\mathrm{COE}}(\tau)$ simulated by a quantum-path integral model.

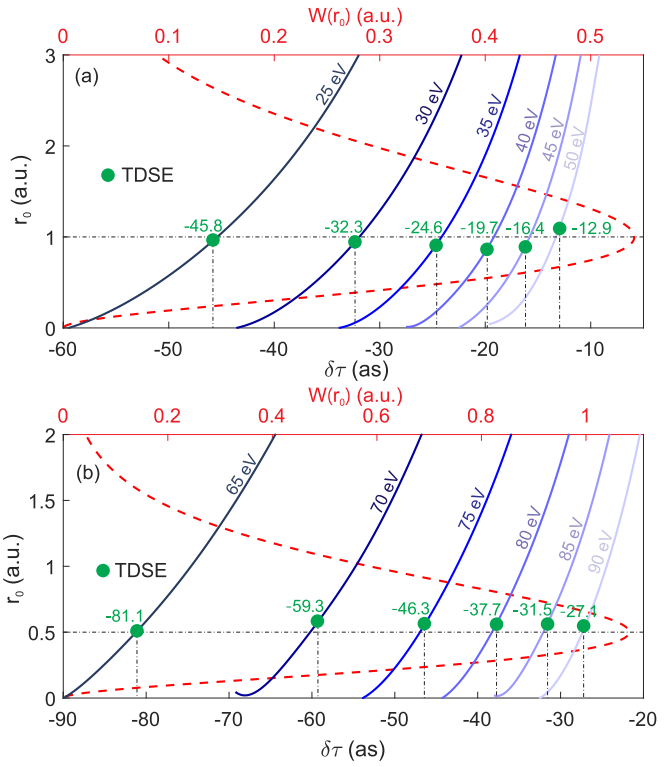

FIG. 3. (a) Classical model predicts photoemission time delays of electrons from the ground state of H atom as a function of initial emission position at XUV photon energies ranging from 25 to 50 eV (solid curves). Also shown are the corresponding TDSE results (green solid circles). (b) Same as in panel (a) but for He^+ and different XUV photon energies ranging from 65 to 90 eV. The red dashed lines represent the radially probability density $W(r_0)$ of the ground states as a function of r_0.

$\varepsilon_{\mathrm{X}} e^{-2\ln(2)(t/T_{\mathrm{X}})^2}\cos(\omega_{\mathrm{X}} t)$ with electric field amplitude ε_{X}, frequency ω_{X}, and pulse duration $T_{\mathrm{X}} = 500$ as. The maximum intensity of the XUV pulse is 1×10^{12} W/cm^2. Both the XUV and IR electric fields are polarized linearly along the z axis. Figure 2(a) shows the quantum-mechanically calculated streaking spectrogram of PEs from the ground state of the H atom in the positive z direction for $\omega_{\mathrm{X}} = 25$ eV. The green solid line in Fig. 2(a) is the corresponding center of energy (COE) $E_{\mathrm{COE}}(\tau)$ (see Appendix A). In the same way, we fit $E_{\mathrm{COE}}(\tau)$ to the analytic function $f(\tau)$ to obtain the photoemission time delay $\delta\tau$. A delay $\delta\tau = -45.8$ as is deduced for $\omega_{\mathrm{X}} = 25$ eV, as shown in the inset in Fig. 2(b).

As the central XUV photon energy increases, the quantum-mechanically calculated photoemission time delay reduces since the Coulomb-laser coupling effect becomes weaker for higher PE kinetic energies [16]. Figure 3(a) shows photoemission delays at different exciting energies of $\omega_{\mathrm{X}} = 25$, 30, 35, 40, 45, and 50 eV. We use these TDSE results as benchmarks for calibrating initial emission positions r_0 in the classical model. To reproduce the same delays, r_0 should be adjusted to 0.96, 0.94, 0.90, 0.92, 0.87, and 1.08, respectively. These six calibrated values yield a mean initial emission position of $\bar{r_0} = 0.95 \pm 0.07$, coinciding with the Bohr radius, the most probable distance between the electron and the nucleus. Our simulation results provide a different understanding for the emission position from a classical trajectory Monte Carlo model [17], which reflects the three-dimensional spatial density distribution of the ground state (the averaged initial position $r_0 = 0$). Our finding contrasts with the choice of the initial emission position in Refs. [18,20], which is inversely proportional to the asymptotical velocity in the absence of the IR field. The excellent agreement between our classical model results and the TDSE results justify the relation between the initial momentum and the initial emission position determined by the law of conservation of energy.

To further validate our findings, we quantum-mechanically calculate the photoemission time delays for the ground state of the He^+ ion, as indicated by the green solid circles in Fig. 3(b). To reproduce the same photoemission delays from TDSE, we should adjust r_0 to 0.51, 0.58, 0.57, 0.55, 0.57, and 0.54 for $\omega_{\mathrm{X}} = 65$, 70, 75, 80, 85, and 90 eV, respectively. A mean initial emission position $\bar{r_0} = 0.55 \pm 0.03$, also coincides with the orbital radius of the ground state for the He^+ ion.

To provide a deep insight into laser-assisted single-photon ionization process and a better understanding of the outcome of our classical model, we developed a quantum-path-integral (QPI) model based on first-order perturbation theory in the velocity gauge. Here we only consider PE trajectories along the positive z axis, since only these PEs can be detected in this direction [18]. We write the amplitude of PE with an asymptotic momentum k as an integration over emission time t and position r,

$$T_k(\tau) \propto \int dt \int r^2 dr \Psi_k^*(r,t) A_X(t) \frac{\partial}{\partial r} \Psi_i(r,t), \qquad (3)$$

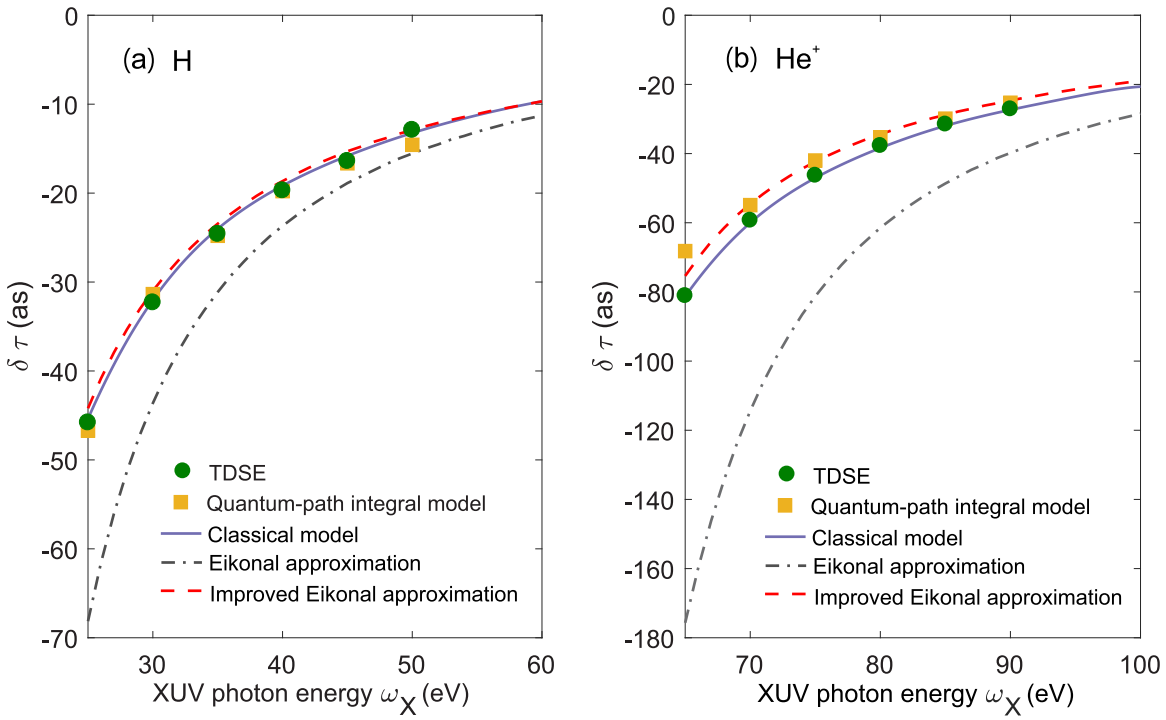

FIG. 4. . Photoemission time delays of electron from the ground states of (a) H atom and (b) He^+ ion as a function of XUV photon energy from TDSE (green solid circles), quantum-path integral model (yellow solid squares), our classical model (purple solid line), the eikonal approximation model (black dot-dashed line), and the improved eikonal approximation model (red dashed line). The initial emission position $r_0 = 1$ for H and 0.5 for He^+ in the last three models.

where $A_X(t)$ is the vector potential of the attosecond XUV pulse and $\Psi_i(r,t) = R(r)e^{iI_p t}$ is the wave function of the initial state. $\Psi_k(r,t) = \frac{1}{r}e^{i[k^2-2V(r)]^{1/2}r+iS_k(r,t)}$ describes the PE wave emitted from position r at time t. The term $S_k(r,t)$ describes the phase accumulated during the emission process, depending on the emission position and emission time. We approximate this phase as the sum of the Volkoff phase and Coulomb-laser coupling phase,

$$S_k(r,t) = S_k^V(t) + S_k^{\mathrm{CL}}(r,t). \tag{4}$$

The Volkoff phase $S_k^V(t) = \int_t^\infty dt'[k + A_{\mathrm{IR}}(t'-\tau)]^2/2$. We obtain the Coulomb-laser coupling phase [16,21]

$$S_k^{\mathrm{CL}}(r,t) = \int_t^\infty dt' V[r_L(t',t,r)], \tag{5}$$

based on the PE trajectory, which is approximated as

$$r_L(t',t,r) = r_L(t'-dt',t,r) + \{\sqrt{k^2 - 2V[r_L(t'-dt',t,r)]} + A_L(t'-dt'-\tau)\}dt'' \tag{6}$$

where $t' = t + ndt'$.

Our QPI model, well reproducing the streaking spectrograms [cf. Figs. 2(a) and 2(c)] and photoemission time delays [cf. circles and squares in Fig. 4] as the TDSE, thus provides complete insights into laser-assisted single-photon transition process from bound states directly into continuum states. The result of spatially coherent superposition of all quantum paths from all possible (continuous) emission positions is equivalent to a quantum path from a certain emission position, in this sense, reproducing the same photoemission time delay.

The measured photoemission delay $\delta\tau$ can be also well understood with an eikonal approximation (EA) model [16], which explicitly reveals its dependence on the CL coupling and IR laser parameters. The energy shift induced by the IR field and the CL coupling in this model is given by [16]

$$\delta E_{\mathrm{COE}}(r_0,\tau) = -k_0 A_{\mathrm{IR}}(\tau) + \frac{V(r_0)}{k_0}A_{\mathrm{IR}}(\tau) - \int_{r_0}^\infty dr' \frac{1}{k_0}A_{\mathrm{IR}}\left(\frac{r'-r_0}{k_0} - \tau\right)\left[-\frac{\partial V(r')}{\partial r'}\right], \tag{7}$$

where $k_0 = \sqrt{2(\omega_X - I_p)}$ and the free-electron classical trajectory $r'(t',t,r_0) = r_0 + k_0(t'-t)$. The last two terms in Eq. (7), describing the CL coupling, indicates reduced coupling effect with increasing k_0. The time shift is induced only by the last term. However, this model overestimates the coupling effect and thus photoemission delays, especially for low kinetic energies and deeper Coulomb potentials (see Fig. 4 and compare the cases for H and He^+), since the momentum of PE is always larger than k_0 in the emission process. Therefore, we can improve this EA model by introducing position-dependent momentum instead of k_0 in the two coupling terms in Eq. (7). The energy shift is then given by

$$\delta E_{\mathrm{COE}}(r_0,\tau) = -k_0 A_{\mathrm{IR}}(\tau) + \frac{V(r_0)}{\frac{k'(r_0)}{2}+\frac{k_0}{2}}A_{\mathrm{IR}}(\tau) - \int_{r_0}^\infty dr' \frac{1}{k'(r')}A_{\mathrm{IR}}\left[\frac{r'-r_0}{\frac{k'(r')}{2}+\frac{k'(r_0)}{2}} - \tau\right]\left[-\frac{\partial V(r')}{\partial r'}\right], \tag{8}$$

where $k'(r') = \sqrt{2[\omega_X - I_p - V(r')]}$. The improved EA model is able to predict photoemission delays at a much better quantitative level, as shown in Figs. 4(a) and 4(b), even for He^+, for which the Coulomb-laser coupling effect is much stronger than that for the H atom. It predicts photoemission delays with an accuracy of 3.5% for the H atom and 7% for the He^+ ion at a low PE kinetic energy near 11 eV.

Quantifying the delays induced solely due to the Coulomb potential of the parent ion in measurement is important to quantitatively investigate photoemission time delays induced by other electronic dynamics using attosecond spectroscopy because CL coupling is inevitable in photoemission process. In the interpretation of emission time delays of PEs from metal surfaces, it usually neglects the CL coupling induced delays near the surface [13,22–27]. In attosecond streaking spectroscopy of diatomic molecules, our classical model is able to evaluate the phase difference of PEs from two centers by calculating their respective classical trajectories, thus predicting the internuclear-distance-dependent yield minimum in streaking spectrograms [28,29]. The electron-electron correlation [4] induced delays are also a result of CL coupling effect but for repulsive Coulomb potential.

We extend our classical model to photoemission from the ground state of the He atom by using the effective one-electron potential [30] and $2p$ excited state of He^+ ion (for calculation details see Appendixes). Our classical model predicts a mean emission position of 0.87 ± 0.15 for the $1s$ state of the He atom, slightly larger than the peak position (0.6) of its radial density. For the $2p$ excited state of the He^+ ion, we must further take into account the polarization effect induced by the IR probing field [31–33] in the classical model. Doing this, the classical model then predicts a mean emission position of 1.23 ± 0.14, smaller than the peak position (2.0) of its radial density. While it is difficult to provide a direct explanation for the coincidence of the determined r_0 with the peak position of the radial density of the ground state of hydrogen-like targets, we can get useful information according to Eq. (3), which indicates r-dependent PE wave amplitude proportional to $r\frac{\partial}{\partial r}R(r)$. For exponential radial functions $R(r)$, this amplitude directly relates to the radial density function of the initial states. For more complicated bound states, this simple relation does not hold any more.

The attosecond streaking spectrum spans over a large energy range due to the broad bandwidth of the exciting XUV pulse. Therefore, we can calculate multiple traces integrated within a relatively narrow energy band, simultaneously within the same streaking spectrogram [34]. Doing this with several streaking spectrograms with energy overlaps, we can obtain the relative change of photoemission time delays as a function of kinetic energies. Such relative change can be used to determine to photoemission position.

In conclusion, we provide comprehensive insights into photoemission time delays measured with attosecond spectroscopy and translate photoemission delays into initial photoemission positions via a classical model. We find that in single-photon ionization, the photoemission position essentially does not depend on the exciting XUV photon energy and the (weak) IR field and coincides with the peak position of the radial density of the ground state for hydrogen-like targets. This work has the potential of advancing attosecond spectroscopy into a promising tool to extract the electronic spatial information with unprecedented resolution.

ACKNOWLEDGMENTS

This work was supported by the National Natural Science Foundation of China (Grants No. 11934006, No. 11674257, No. 11627809, No. 12021004, and No. 11947096), Hubei Provincial Department of Education (Grant No. T201806), the Natural Science Foundation of Hubei Province (Grant No. 2020CFA082), and the Guangdong Major Project of Basic and Applied Basic Research (Grant No. 2019B030302003).

APPENDIX A: NUMERICAL SOLUTION OF TIME-DEPENDENT SCHRöDINGER EQUATION

The time-dependent Schrödinger equation (TDSE) in spherical polar coordinates with azimuthal symmetry is [35]

$$i\frac{\partial \Psi(\mathbf{r},t)}{\partial t} = \left[-\frac{1}{2}\frac{\partial^2}{\partial r^2} + \frac{l(l+1)}{2r^2} + V(r) + F(r,t)\right]\Psi(\mathbf{r},t), \tag{A1}$$

where $\Psi(\mathbf{r},t) = r\Phi(\mathbf{r},t)$ is the reduced wave function. $\Phi(\mathbf{r},t) = \sum_{l=0}^{l_{\max}} \mathrm{R}_l(r,t)P_l(\cos\theta)$ with $\mathrm{R}_l(r,t)$ and $P_l(\cos\theta)$ of the radial wave functions and the normalized Legendre polynomials, respectively. l is the angular quantum number. $F(r,t) = [E_{\mathrm{IR}}(t-\tau) + E_X(t)]r\cos\theta$ is the interaction between electrons with the XUV and IR electric fields polarized linearly along the z axis. The maximum of angular quantum number $l_{\max}$ is set to 19, large enough to guarantee converged simulation results. The spatial step $dr = 0.0365$ and the time step $dt = 0.0013$ yield photoemission time delays with an accuracy less than 0.1 as. We solve Eq. (A1) using the split-operator method and then directly project the final electron wave packet $\Psi(\mathbf{r},t_f)$ onto the scattering state $\Psi_{k_f}^{(-)}(\mathbf{r})$ with an asymptotic momentum k (emission angle θ_k), to obtain a τ-dependent photoelectron momentum distribution,

$$P_k(k,\theta_k,\tau) = |\langle \Psi_k^{(-)}(\mathbf{r})|\Psi(\mathbf{r},t_f)\rangle|^2. \tag{A2}$$

Here, $\Psi_k^{(-)}(\mathbf{r}) = \sum_{l=0}^{l_{\max}} e^{i[l\pi/2-\sigma_l(k)-\delta_l(k)]}\frac{F_{kl}(r)}{kr}P_l^{\star}(\theta_k)P_l(\theta)$ [36], $F_{kl}(r) = \sqrt{2/\pi}\sin[kr - \eta\ln(2kr) - l\pi/2 + \sigma_l(k) + \delta_l(k)]$. $\eta = -Z/k$ and $\sigma_l(k) = \arg[\Gamma(l+1-iZ/k)]$ are the Coulomb parameter and Coulomb phase shift, respectively [37,38]. The non-Coulombic phase shift $\delta_l(k)$ is zero for pure Coulomb potentials. If the potential $V(r)$ contains an additional short-range potential, but is Coulombic at asymptotic distances, i.e., $V(r) = -Z/r$ for $r \to \infty$, an additional phase shift $\delta_l(k)$ should be added in F_{kl}. This non-Coulombic phase shift $\delta_l(k)$ can be obtained by numerical methods [39]. The photoelectron energy distribution is then calculated by [40]

$$P_E(E,\theta_k,\tau) = 2\pi k P_k(k,\theta_k,\tau), \tag{A3}$$

with $E = k^2/2$. The centers of energy (COE) of the streaking spectrogram of photoelectrons emitted in the positive z direction is defined as

$$E_{\mathrm{COE}}(\tau) = \frac{\int E P_E(E,\theta_k=0,\tau)dE}{\int P_E(E,\theta_k=0,\tau)dE}. \tag{A4}$$

APPENDIX B: STREAKING PHOTOEMISSION TIME DELAYS FOR HE ATOMS IN SINGLE-ACTIVE-ELECTRON APPROXIMATION

We calculate the streaking photoemission time delays from the ground state ($1s$) of He atoms using the effective one-electron potential from Ref. [30]:

$$V(r) = -\frac{1 + a_1 e^{-a_2 r} + a_3 r e^{-a_4 r} + a_5 e^{-a_6 r}}{r}, \quad \text{(B1)}$$

with $a_1 = 1.231$, $a_2 = 0.662$, $a_3 = -1.325$, $a_4 = 1.236$, $a_5 = -0.231$, and $a_6 = 0.480$. The photoemission time delays from TDSE simulated streaking spectrograms of this atomic potential are -20.1, -13.8, -10.6, -8.5, -6.8, and -5.7 as at exciting XUV photon energies of $\omega_X = 50$, 60, 70, 80, 90, and 100 eV. The photoemission time delays calculated using this effective one-electron model potential are almost the same as those from another effective one-electron model potential [4]. They also coincide with the two-electron TDSE results if the ion is left in its ground state for final kinetic energies under consideration [31], suggesting no significant influence of electronic correlation on the photoemission time delays in this case.

APPENDIX C: INCLUDING POLARIZATION EFFECT IN THE CLASSICAL MODEL

In laser-assisted single-photon photoionization from $2p$ excited state of He^+ ion, the interaction of the initial-state permanent dipole prior to photoionization with the IR-laser field leads to a time-dependent ionization potential shift [31–33]

$$\Delta Ip(\tau) = \vec{d} \cdot \vec{E}_{\rm IR}(\tau), \quad \text{(C1)}$$

where $\vec{d}$ is the dipole moment. In our classical model, this energy shift is included in the ionization potential I_p in Eq. (2) of the main text. Then, our classical model predicts $r0 = 1.24$, 1.07, 1.27, 1.35, 1.27, and 1.2 at XUV photon energies 25, 30, 40, 50, 60, and 70 eV, in order to reproduce TDSE calculated photoemission time delays -37.8, -25.1, -10.4, -2.2, 1.9, and 4.6 as, respectively.

[1] M. Schultze, M. Fieß, N. Karpowicz, J. Gagnon, M. Korbman, M. Hofstetter, S. Neppl, A. L. Cavalieri, Y. Komninos, Th. Mercouris *et al.*, Science **328**, 1658 (2010).

[2] K. Klünder, J. M. Dahlström, M. Gisselbrecht, T. Fordell, M. Swoboda, D. Guénot, P. Johnsson, J. Caillat, J. Mauritsson, A. Maquet, R. Taïeb, and A. L'Huillier, Phys. Rev. Lett. **106**, 143002 (2011).

[3] P. M. Paul, E. S. Toma, P. Breger, G. Mullot, F. Augé, Ph. Balcou, H. G. Muller, and P. Agostini, Science **292**, 1689 (2001).

[4] M. Ossiander, F. Siegrist, V. Shirvanyan, R. Pazourek, A. Sommer, T. Latka, A. Guggenmos, S. Nagele, J. Feist, J. Burgdörfer, R. Kienberger, and M. Schultze, Nat. Phys. **13**, 280 (2017).

[5] M. Isinger, R. J. Squibb, D. Busto, S. Zhong, A. Harth, D. Kroon, S. Nandi, C. L. Arnold, M. Miranda, J. M. Dahlström *et al.*, Science **358**, 893 (2017).

[6] G. Schmid, K. Schnorr, S. Augustin, S. Meister, H. Lindenblatt, F. Trost, Y. Liu, N. Stojanovic, A. Al-Shemmary, T. Golz *et al.*, Phys. Rev. Lett. **122**, 073001 (2019).

[7] J. Feist, O. Zatsarinny, S. Nagele, R. Pazourek, J. Burgdörfer, X. Guan, K. Bartschat, and B. I. Schneider, Phys. Rev. A **89**, 033417 (2014).

[8] J. Vos, L. Cattaneo, S. Patchkovskii, T. Zimmermann, C. Cirelli, M. Lucchini, A. Kheifets, A. S. Landsman, and U. Keller, Science **360**, 1326 (2018).

[9] A. Chacon and C. Ruiz, Opt. Express **26**, 4548 (2018).

[10] A. Chacon, M. Lein, and C. Ruiz, Phys. Rev. A **89**, 053427 (2014).

[11] C. Ott, A. Kaldun, P. Raith, K. Meyer, M. Laux, J. Evers, C. H. Keitel, C. H. Greene, and T. Pfeifer, Science **340**, 716 (2013).

[12] J. Fuchs, N. Douguet, S. Donsa, F. Martin, J. Burgdörfer, L. Argenti, L. Cattaneo, and U. Keller, Optica **7**, 154 (2020).

[13] Z. Tao, C. Chen, T. Szilvási, M. Keller, M. Mavrikakis, H. Kapteyn, and M. Murnane, Science **353**, 62 (2016).

[14] Q. Liao, W. Cao, Q. Zhang, K. Liu, F. Wang, P. Lu, and U. Thumm, Phys. Rev. Lett. **125**, 043201 (2020).

[15] F. Siek, S. Neb, P. Bartz, M. Hensen, C. Strüber, S. Fiechter, M. Torrent Sucarrat, V. M. Silkin, E. E. Krasovskii, N. M. Kabachnik *et al.*, Science **357**, 1274 (2017).

[16] C.-H. Zhang and U. Thumm, Phys. Rev. A **82**, 043405 (2010).

[17] S. Nagele, R. Pazourek, J. Feist, K. Doblhoff-Dier, C. Lemell, K. Tőkési, and J. Burgdörfer, J. Phys. B: At., Mol. Opt. Phys. **44**, 081001 (2011).

[18] M. Ivanov and O. Smirnova, Phys. Rev. Lett. **107**, 213605 (2011).

[19] D. Kiesewetter, R. R. Jones, A. Camper, S. B. Schoun, P. Agostini, and L. F. DiMauro, Nat. Phys. **14**, 68 (2018).

[20] J. M. Dahlström, D. Guénot, K. Klünder, M. Gisselbrecht, J. Mauritsson, A. L'Huillier, A. Maquet, and R. Taïeb, Chem. Phys. **414**, 53 (2011).

[21] O. Smirnova, M. Spanner, and M. Ivanov, J. Phys. B: At., Mol. Opt. Phys. **39**, S323 (2006).

[22] A. L. Cavalieri, N. Müller, Th. Uphues, V. S. Yakovlev, A. Baltuška, B. Horvath, B. Schmidt, L. Blümel, R. Holzwarth, S. Hendel *et al.*, Nature (London) **449**, 1029 (2007).

[23] S. Neppl, R. Ernstorfer, E. M. Bothschafter, A. L. Cavalieri, D. Menzel, J. V. Barth, F. Krausz, R. Kienberger, and P. Feulner, Phys. Rev. Lett. **109**, 087401 (2012).

[24] Q. Liao and U. Thumm, Phys. Rev. Lett. **112**, 023602 (2014).

[25] Q. Liao and U. Thumm, Phys. Rev. A **92**, 031401(R) (2015).

[26] R. Locher, L. Castiglioni, M. Lucchini, M. Greif, L. Gallmann, J. Osterwalder, M. Hengsberger, and U. Keller, Optica **2**, 405 (2015).

[27] L. Kasmi, M. Lucchini, L. Castiglioni, P. Kliuiev, J. Osterwalder, M. Hengsberger, L. Gallmann, P. Krüger, and U. Keller, Optica **4**, 1492 (2017).

[28] Q.-C. Ning, L.-Y. Peng, S.-N. Song, W.-C. Jiang, S. Nagele, R. Pazourek, J. Burgdörfer, and Q. Gong, Phys. Rev. A **90**, 013423 (2014).

[29] F. Wang, K. Liu, X. Zhang, Z. Wang, M. Qin, Q. Liao, and P. Lu, Phys. Rev. A **100**, 043405 (2019).
[30] X. M. Tong and C. D. Lin, J. Phys. B: At., Mol. Opt. Phys. **38**, 2593 (2005).
[31] R. Pazourek, S. Nagele, and J. Burgdörfer, Rev. Mod. Phys. **87**, 765 (2015).
[32] J. C. Baggesen and L. B. Madsen, Phys. Rev. Lett. **104**, 043602 (2010).
[33] R. Pazourek, S. Nagele, and J. Burgdörfer, Faraday Discuss. **163**, 353 (2013).
[34] L. Seiffert, Q. Liu, S. Zherebtsov, A. Trabattoni, P. Rupp, M. C. Castrovilli, M. Galli, F. Süßmann, K. Wintersperger, J. Stierle *et al.*, Nat. Phys. **13**, 766 (2017).
[35] M. R. Hermann and J. A. Fleck, Jr., Phys. Rev. A **38**, 6000 (1988).
[36] H. Park and R. N. Zare, J. Chem. Phys. **104**, 4554 (1996).
[37] M. Aymar and M. Crance, J. Phys. B: At. Mol. Phys. **13**, L287 (1980).
[38] M. Edwards, X. Tang, and R. Shakeshaft, Phys. Rev. A **35**, 3758 (1987).
[39] K. Pachucki, D. Leibfried, and T. W. Hänsch, Phys. Rev. A **48**, R1(R) (1993).
[40] X.-F. Hou, L.-Y. Peng, Q.-C. Ning, and Q. Gong, J. Phys. B: At., Mol. Opt. Phys. **45**, 074019 (2012).